Behavioral/Cognitive

Changes in White Matter Microstructure Impact Cognition by Disrupting the Ability of Neural Assemblies to Synchronize

Sonya Bells,[1] Jérémie Lefebvre,[7,10] Steven A. Prescott,[1,9] Colleen Dockstader,[6] Eric Bouffet,[2,5] Jovanka Skocic,[1] Suzanne Laughlin,[3,8] and Donald J. Mabbott[1,4]

[1]Neurosciences and Mental Health, [2]Division of Haematology/Oncology, [3]Diagnostic Imaging, The Hospital for Sick Children, Toronto, Ontario M5G 1X8, Canada, and Departments of [4]Psychology, [5]Paediatrics, [6]Human Biology Program, [7]Mathematics, [8]Medical Imaging, [9]Physiology and Institute of Biomaterials and Biomedical Engineering, University of Toronto, Toronto, Ontario M5S 1A1, Canada, and [10]Krembil Research Institute, University Health Network, Toronto, Ontario M5G 2C4, Canada

Cognition is compromised by white matter (WM) injury but the neurophysiological alterations linking them remain unclear. We hypothesized that reduced neural synchronization caused by disruption of neural signal propagation is involved. To test this, we evaluated group differences in: diffusion tensor WM microstructure measures within the optic radiations, primary visual area (V1), and cuneus; neural phase synchrony to a visual attention cue during visual-motor task; and reaction time to a response cue during the same task between 26 pediatric patients (17/9: male/female) treated with cranial radiation treatment for a brain tumor (12.67 ± 2.76 years), and 26 healthy children (16/10: male/female; 12.01 ± 3.9 years). We corroborated our findings using a corticocortical computational model representing perturbed signal conduction from myelin. Patients show delayed reaction time, WM compromise, and reduced phase synchrony during visual attention compared with healthy children. Notably, using partial least-squares–path modeling we found that WM insult within the optic radiations, V1, and cuneus is a strong predictor of the slower reaction times via disruption of neural synchrony in visual cortex. Observed changes in synchronization were reproduced in a computational model of WM injury. These findings provide new evidence linking cognition with WM via the reliance of neural synchronization on propagation of neural signals.

Key words: **cognition; diffusion MRI; information processing speed; MEG; neural synchrony; white matter**

Significance Statement

By comparing brain tumor patients to healthy children, we establish that changes in the microstructure of the optic radiations and neural synchrony during visual attention predict reaction time. Furthermore, by testing the directionality of these links through statistical modeling and verifying our findings with computational modeling, we infer a causal relationship, namely that changes in white matter microstructure impact cognition in part by disturbing the ability of neural assemblies to synchronize. Together, our human imaging data and computer simulations show a fundamental connection between WM microstructure and neural synchronization that is critical for cognitive processing.

Introduction

Despite the robust association between cognition and the microstructure of white matter (WM), very little is known about the neurophysiological basis for that link (Fields, 2015). Recently, it has been proposed that WM affects cognition by coordinating the timing of neuronal signaling to maintain oscillatory synchronization within and between neural coalitions (Pajevic et al., 2014; Fields, 2015; Nunez et al., 2015). Although this hypothesis has been modeled in simple oscillatory circuits and tested in animals (Salami et al., 2003; Pajevic et al., 2014), to our knowledge it has not been examined in the context of large-scale network models or tested

Received Feb. 28, 2017; revised July 11, 2017; accepted July 14, 2017.

Author contributions: J.L., C.D., and D.J.M. designed research; S.B., J.L., C.D., E.B., and D.J.M. performed research; S.B., J.L., S.A.P., J.S., S.L., and D.J.M. analyzed data; S.B., J.L., S.A.P., C.D., E.B., J.S., S.L., and D.J.M. wrote the paper.

This work was supported by operating grants from by the Canadian Institutes of Health Research, the Pediatric Oncology Group of Ontario, Brain Canada, and the Garron Family Cancer Centre at the Hospital for Sick Children. We thank Iska Moxon-Emre for proofreading and statistical support.

The authors declare no competing financial interests.

Correspondence should be addressed to Dr. Donald J. Mabbott, Neurosciences and Mental Health, The Hospital for Sick Children, 686 Bay Street, Toronto, ON M5G 0A4, Canada. E-mail: donald.mabbott@sickkids.ca.

DOI:10.1523/JNEUROSCI.0560-17.2017

 0270-6474/17/378227-12$15.00/0

in humans. Such work is critical for understanding how WM may influence neural network communication and human cognition.

Prior studies have focused on the relations between WM microstructure and neurophysiological measures without considering behavioral measures of cognition (Roberts et al., 2009; Hindriks et al., 2015; Nazem-Zadeh et al., 2016). For example, increased organization of WM microstructure predicts decreased latency of the evoked visual response in infants, children, and healthy adults (Dubois et al., 2008; Stufflebeam et al., 2008; Dockstader et al., 2012). WM maturation accounts for age-related increases in the speed of this visual response (Dubois et al., 2008; Dockstader et al., 2012) and WM compromise corresponds with reduced neural response in multiple disorders (Sponheim et al., 2011; Stephen et al., 2013; Garcés et al., 2014). How these relations combine and impact cognition is unknown however.

Here, we ask whether WM affects an important cognitive function, *visual information processing speed*, via effects on neural synchronization in a sample of children treated for a brain tumor (BT) and healthy children. Information processing speed is the rate of completing cognitive operations and is critical for higher-order cognitive functions (Kail, 2000; Ferguson and Bowey, 2005) The organization of WM microstructure predicts the speed of information processing in healthy children (Mabbott et al., 2006) and adults (Madden et al., 2004), and in many neurological disorders (Soria-Pastor et al., 2008; Bethune et al., 2011; Scantlebury et al., 2016). Children treated for BT, including with cranial radiation treatment (CRT) exhibit long-term cognitive impairment, including deficits in information processing speed (Mabbott et al., 2006, 2009; Law et al., 2015). Notably, tumors and their treatment with radiation damages WM (Mabbott et al., 2006; Nieder et al., 2007). Both WM insult and disrupted neuronal activation in BT patients independently predict slowed information processing speed (Dockstader et al., 2014; Scantlebury et al., 2016). The neurophysiologic mechanisms that underlie these relations, particularly how structural compromise manifests as cognitive impairment, are poorly understood.

We tested not only whether altered WM microstructure was correlated with reduced visual information processing speed, but also whether those changes were mediated by reduced neural synchronization within neural populations. We measured WM microstructure using diffusion tensor imaging (DTI) within areas involved in early visual procession and a control region not related to this function, the frontal lobe. WM regions involved in early visual processing include the optic radiations (ORs) and WM underlying V1 and cuneus (Mori et al., 2008; De Moraes, 2013). The early visual response typically shows robust synchrony and strong phase-locking to a visual cue during a visual attention task (Siegel et al., 2008) and this neural synchronization was assessed using magnetoencephalography (MEG). Specifically, synchrony within canonical frequency bands was quantified as trial-to-trial phase-locking in cortical regions, such as V1 and cuneus, known to be activated during visual attention. Phase-locking is a measure of temporal synchronization of neural signals to an external stimulus, in our case, the visual attention cue (Lachaux et al., 1999). Notably, the magnitude of visual cortex low-frequency band (i.e., theta/delta/alpha) phase-locking in response to a visual attention cue predicts visual-motor task performance (Yamagishi et al., 2008). To measure cognition we operationalized information processing speed as reaction time of a button press in response to the "go" stimulus after the attention cue was displayed. Such tasks have been used effectively to assess age-related changes in information processing speed (Western and Long, 1996; Konrad et al., 2009). Finally, we used computer simulations to further explore the hypothesis that perturbed axonal communication due to WM damage may be responsible for disruption of phase synchrony.

Table 1. Participant characteristics and medical variables

	Patients ($n = 26$)	Healthy control ($n = 26$)	p value
Sex (male)	16	17	0.84
Handedness (right)	23	24	0.64
Age at assessment, years			
Mean	12.67	12.01	0.54
SD	2.76	3.9	
Range	7.90–18.81	5.15–18.93	
Age at diagnosis, years			
Mean	6.81	—	—
SD	2.34	—	
Range	2.58–11.59	—	
Time from diagnosis to assessment, years			
Mean	5.86	—	—
SD	3.43	—	
Range	1.10–14.43	—	
Tumor type			—
Anaplastic Astrocytoma	1	—	
Ependymoma	4	—	
Medulloblastoma	21	—	
Tumor location			
Supra tentorial	1	—	—
Infratentorial	25	—	
No. of surgeries			—
1	17	—	
2	4	—	
3	1	—	
Radiation type			—
Focal (54–59.4 Gy) to tumor	3	—	
Focal (54–59.4 Gy) to tumor then cranial-spinal at recurrence (36 Gy)	2		
Cranial-spinal (23.4–36 Gy) + boost (18–32.4 Gy)	21	—	
Treated with chemotherapy	25	—	—
Hydrocephalus			—
No hydrocephalus	14	—	
Hydrocephalus with no treatment	4	—	
Hydrocephalus requiring CSF diversion	9	—	
Scanner Type			
GE LX 1.5T MRI	14	11	0.41
Siemens 3T	12	15	
Mean SNR GE LX 1.5T MRI	12.52	9.88	0.52
Mean SNR Siemens 3T	33.70	29.19	
DTI indices for OR			
Mean fractional anisotropy	0.41	0.43	0.000
SD	0.04	0.03	
Mean diffusivity	0.00083	0.00079	0.001
SD	0.00004	0.00003	
Mean axial diffusivity	0.00121	0.00119	0.110
SD	0.00005	0.00005	
Mean radial diffusivity	0.00064	0.00059	0.000
SD	0.00006	0.00005	

Materials and Methods

Participants

Participants were 26 healthy children and 26 pediatric patients treated for a posterior fossa BT (either medulloblastoma or ependymoma) at The Hospital for Sick Children (see Table 1 for sample characteristics). Informed written consent (or assent and consent from a parent for younger children) was obtained by all participants and the hospital's Research Ethics Board approved the study. Eligible patients were identified through database review, which included those diagnosed with a malig-

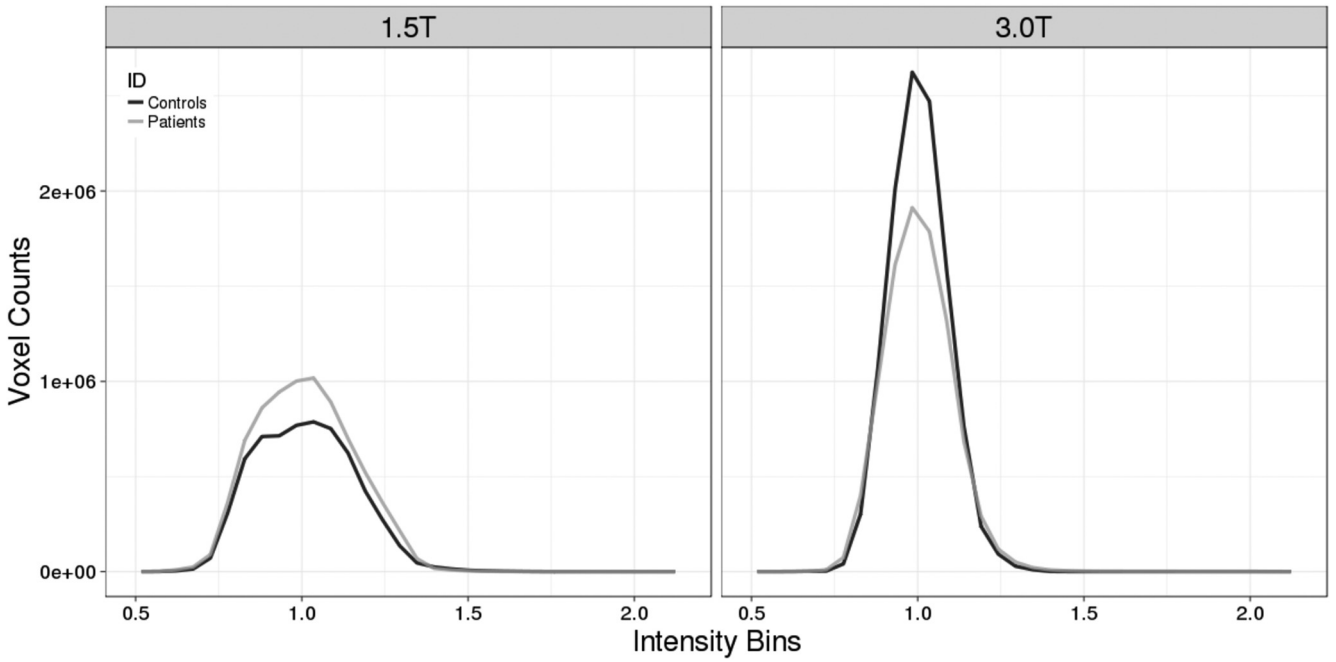

Figure 1. Bias field histograms at 1.5 and 3 T for patient and healthy control children.

nant BT and having received CRT. All patients were seen 12 or more months following treatment. Patients were not recruited if they had a diffuse brainstem glioma, were receiving palliative care, or had a premorbid history of neurological/learning disability. Although the majority of BT patients were treated with whole-brain radiation (90%), three patients received focal radiation: two of these patients had radiation limited to the tumor bed. There were no significant differences between groups with respect to age ($F_{(1,50)} = 0.51$, $p > 0.05$), sex ($\chi^2_{(1,n=52)} = 0.22$, $p > 0.05$), or scanner type used for MRI ($\chi^2_{(1,n=52)} = 0.69$, $p > 0.05$). Detailed medical variables of the patients treated for BT and participant characteristics can be found in Table 1.

MRI methods

We collected both T1-weighted and diffusion tensor images for WM microstructure assessment and registration purposes. DTI is an indirect measure of WM microstructure and that reflects the fact that axons (including axon diameter and myelin) create coherent obstacles to water diffusion and thus reveals orientation dependency (Basser et al., 1994). We characterized directional dependency, and thus WM microstructure, using MRI by scalar indices such as radial diffusivity (RD), axial diffusivity (AD), mean diffusivity (MD), and fractional anisotropy (FA) within the optic radiations.

MRI recordings. T1-weighted images were acquired with a GE LX 1.5T MRI scanner (GE Healthcare) using a 3D FSPGR protocol (TR/TE = 10.056/4.2 ms, 124 contiguous axial slices, 1.5 mm thick, 256 ×192 mm matrix) and single-shot spin echo diffusion-weighted sequence [31 directions, 1 *b*0 image, *b* value = 1000 s/mm^2, TR = 15,000 ms, TE = 95.4 ms (min), flip angle = 90°, slice thickness = 3 mm, matrix = 128 × 128 and interpolated to 256 × 256 mm, 45–52, encoding direction = A/P] or a Siemens 3T scanner using a 3D MPRAGE Grappa 2 protocol (TR/TE = 2300/3.91 ms, 160 contiguous slices, 1 mm thick, 256 × 224 mm matrix) and a single-shot spin echo diffusion-weighted sequence [30 directions, 1 *b*0 image, *b* value = 1000 s/mm2, TR = 9000 ms, TE = 90 ms (min), flip angle = 90°, slice thickness 2 mm, matrix = 122 × 122 mm and interpolated to 244 × 244 mm, 70 slices, encoding direction = A/P]. Children watched a movie through video goggles to prevent excessive head movement during the scan. To overlay MEG information on the MRI of the subject's brain, the three fiducial points were identified on MRI images and coregistered with the fiducial information from the MEG.

Signal-to-noise differences are present in diffusion data collected with these magnet strengths (Law et al., 2015). Hence, we calculated signal-to-noise ratio (SNR) for a region-of-interest (ROI) within the occipital lobe (mean number of voxels = 323) for all participants across all gradient directions. As expected, SNR was greater for participants scanned at 3T versus 1.5T (31.44 vs 11.20; $F_{(1,48)} = 197.05$, $p = 0.000$, ANOVA,). Because we matched the groups by scanner type, we observed no interaction between group (patients vs healthy children) and scanner type in SNR ($F_{(1,48)} = 0.42$, $p = 0.52$, ANOVA; see Table 1 for SNR). We also calculated the bias fields for the diffusion sequences at both 1.5 and 3T across all participants. The distribution of intensities in the bias fields were similar between patients and controls within each respective-field strength (Fig. 1). To ensure that scanner type was not a confound, we controlled for this variable in our analyses of group differences in DTI indices.

MRI data preprocessing. DTI data were eddy-current corrected and FA, RD, MD, and AD maps were calculated using FSL software (Smith et al., 2006). FA maps were nonlinearly aligned to each other to identify the most representative image, a study-specific target, which was then linearly registered into MNI152 space (MNI152; Montreal Neurological Institute). All images were then aligned to the MNI152 standard space, via registration through the target image, and a mean FA map was created. Subsequently, a cross-subject skeleton map was generated using this mean FA map, thresholded at FA >0.2 to include only the large fiber tracts. Finally, individual DTI maps (FA, RD, MD, and AD) were projected onto the skeleton and only the maximum values along the width of each large fiber tract were considered in subsequent analyses. This is known as tract-based spatial statistics (TBSS; Smith et al., 2006) whereby it applies a voxelwise statistical approach to assess WM architecture.

WM networks. We used FSL software to create three WM ROIs on the DTI maps of every participant: (1) a region known to be involved in early visual processing including optic radiations, and WM underlying V1 and the cuneus (OR/V1/Cuneus) in the right hemisphere (Mori et al., 2008); (2) the same region in the left hemisphere; and (3) a control region within the right frontal lobe. We chose this control region since it is not closely associated with early visual processing and we used it to test the specificity of brain-behavioral relations in our partial least-squares (PLS) path models. We extracted the averaged value for FA, RD, MD, and AD indices for these regions.

MEG methods

We used a whole-head 151 channel CTF MEG system (VSM MedTech) to measure differences in oscillatory phase-locking associated to an "at-

tend" cue during a visual-motor reaction task between patients and healthy children.

Visual-motor reaction time paradigm. For the duration of the visual-motor reaction task, participants were asked to keep their eyes open and fixated on a computer screen. Their dominant hand was resting at their side with their thumb gently resting on a button of a nonmagnetic fiber-optic response pad. A black cross first appeared onscreen as an "attentional" cue to signify an impending visual stimulus. This was the attend cue to which our MEG variables were derived. The black cross remained on-screen for 1.5–2.5 s (exact onset was randomly jittered), requiring participants to maintain attention in this central location until the appearance of a green visual "go" stimulus, which was accompanied with a visual gradient in the lower-right visual field. Participants were instructed to push the button with their dominant thumb as soon as the go stimulus appeared. Once they pushed the button the attend cue would reappear within 1 s. Each participant received 100 trials. We extrapolated the button press latencies for each participant, for each trial, and calculated the average reaction time latency for each individual.

MEG recordings. Neuromagnetic activity was recorded in a magnetically shielded room and a third-order synthetic gradiometer correction was applied to reduce noise. Participant head location was continuously recorded and monitored using three magnetic coils placed at the nasion and preauricular points. Continuous MEG data were acquired while the participants lay supine in the MEG at a rate of 1250 samples/s and bandpass filtered at 0–300 Hz, while small coils placed at fiducial locations (nasion and pre-auricular points) were used to monitor head position during recording. Participants fixated on a semitransparent screen placed 50 cm from their eyes and eye blinks and saccades were monitored with electro-oculograms applied just distal to the lateral canthus of each eye, and one on the left mastoid process. Upon completion of MEG data collection, the coils were replaced with MRI-visible markers for coregistration between MEG and MRI information.

MEG data preprocessing

Data were off-line filtered from 1 to 100 Hz and segmented into epochs from −100 to 1000 ms, with respect to the "attended" cue. Each epoch was visually inspected and contaminated trials due to eye blinks or gross muscle movement were removed before beamformer analysis. Localization of brain activity was conducted using event-related beamformer (ERB) algorithms using a 2 mm grid for each participant using Brain Wave software (Cheyne, 2012). Forward solutions were based on the single sphere model fit to the inner skull surface. To combine source localization results across participants, ERB images were spatially normalized with statistical parametric mapping (SPM; Ashburner, 2009) using Brain Wave integrated software and registered to the SPM template. The anatomical sources of neural activity for time points (1–100, 101–200, 201–300, and 301–400 ms) provide current magnitudes for further analysis.

MEG ROI. Statistically significant ERB images for each group separately were averaged and thresholded using a nonparametric permutation test adapted for beamformer source images (Singh et al., 2003) and glass-heads were created to visually inspect the peak sources related to visual attention within each active window. We then evaluated ERB images for each participant using anatomically predefined ROI vertices within the occipital lobe. This method is a desirable method when activity is weak as in our patient population that can be overlooked in whole-brain methods after statistical thresholding. We defined two regions known for early visual attention (Simpson et al., 2011) for our paradigm: right V1 (15, −69, 8) and right cuneus (36, −86, 18; in Talairach space, mm). To determine the flow of activation between the two areas we determined the initial onset of activity (when the mean is 2 SD above baseline) for V1 and cuneus.

Phase-locking factor in ROIs. Talairach coordinates for each peak were unwarped to the largest peak within a 5 mm radius in individual space using Brain Wave software to obtain individual virtual sensors from the scalar beamformer. Single-trial source activity waveforms for each virtual sensor were used for time-frequency analysis using a Morlet waved-based technique across the time series and over the 1–60 Hz frequency range, with center frequencies at 0.5 Hz intervals, to determine the phase synchrony or "intertrial" coherence known as the phase-locking factor (PLF). The PLF is an amplitude-independent index of phase synchrony and reflects the variability of oscillatory activity across multiple trials at a particular time-frequency point following an event (Tallon-Baudry et al., 1996). The PLF is scaled from "0" reflecting no phase synchrony (completely random phase of activity) to "1" reflecting no phase variability (activity is perfectly synchronized in phase). Phase-locking plots for the two ROIs were averaged across participants within each group. We then identified peak PLFs for each participant, in each location, in the following frequency bands: delta (2–4 Hz), theta (5–7 Hz), alpha (8–15 Hz), beta (16–29 Hz), and gamma (30–60 Hz). We then conducted a multivariate analysis comparing patients versus healthy children across all frequency bands for right V1 and cuneus.

Table 2. Model parameters for computational model

Symbol	Definition	Value
α_e	Membrane rate constant: excitatory cortical cells	1.0
α_i	Membrane rate constant: inhibitory cortical cells	1.3
α_{V5}	Membrane rate constant: cuneus cells	1.0
$w_{e,e}$	e ⟶ e synaptic connection strength	1.6
$w_{e,i}$	e ⟶ i synaptic connection strength	2.0
$w_{i,e}$	i ⟶ e synaptic connection strength	−3.6
$w_{i,i}$	i ⟶ i synaptic connection strength	−0.1
$w_{e,V5}$	Cortex ⟶ cuneus synaptic connection strength	2.0
i_e	Bias input to excitatory population	0.0
i_i	Bias input to excitatory population	−0.2
h	Activation function threshold	0.0
β	Activation function gain	25
D	Intrinsic noise level	0.001
dt	Integration time step	1 ms

Experimental design and statistical analyses

Group differences. We examined differences reaction time between in patients and healthy children using a two-sample *t* test. To compare WM microstructure between groups, we used a voxelwise approach with TBSS to test for group differences in DTI indices across the entire brain (Smith et al., 2006) and controlling for scanner. Group differences for each index were determined using cross-subject voxelwise statistics. Results were corrected for multiple comparisons using a threshold-free cluster enhancement and threshold at an alpha level of 0.05. Clusters of significant group differences for each DTI index were visualized as an overlay on FSL's FA template. We then conducted a 2 (group: patients vs controls) × 2 (hemisphere: left vs right) multivariate ANOVA with repeated measures on the last variable across DTI indices (FA, MD, RD, AD) extracted from the OR/V1/cuneus/ ROIs, also controlling for scanner. Finally, a 2 (group: patients vs controls) × 2 (right V1, right cuneus) × 5 (frequency band: delta, theta, alpha, beta, gamma) ANOVA with repeated measures on the last two variables was conducted on PLF. Statistical tests were two-tailed, and an alpha-level of $p < 0.05$ was used to determine significance.

PLS–path modeling. We used PLS–path model analysis, using PLSpm in R to measure the performance of our path model (number of bootstraps = 5000; Sanchez, 2013) For this model, we hypothesize that treatment for a BT had direct and indirect effects on reaction time via WM microstructure compromise and visual cortex neuronal synchrony. We first tested the accuracy of measurement model using a number of criteria. The accuracy of the measured model was estimated by examining the relationship between the latent constructs and their associated measures, known as loading. We also tested how well each measure corresponded to their latent constructs using Cronbach's alpha and Dillon–Goldstein's rho. Finally, the discriminant validity of the measurement model was tested by evaluating whether the cross-loading for each measure relative to the other latent constructs were larger than the loadings obtained from measures belonging to other latent constructs. Next, the quality of the structural model was evaluated in four ways: (1) significance of the regression fit (*t* test), (2) R^2 determination coefficients of the endogenous variables (low $R < 0.2$, moderate $0.2 < R < 0.5$), (3) average variance extracted (AVE), and (4) goodness-of-fit (GoF). The GoF measure for

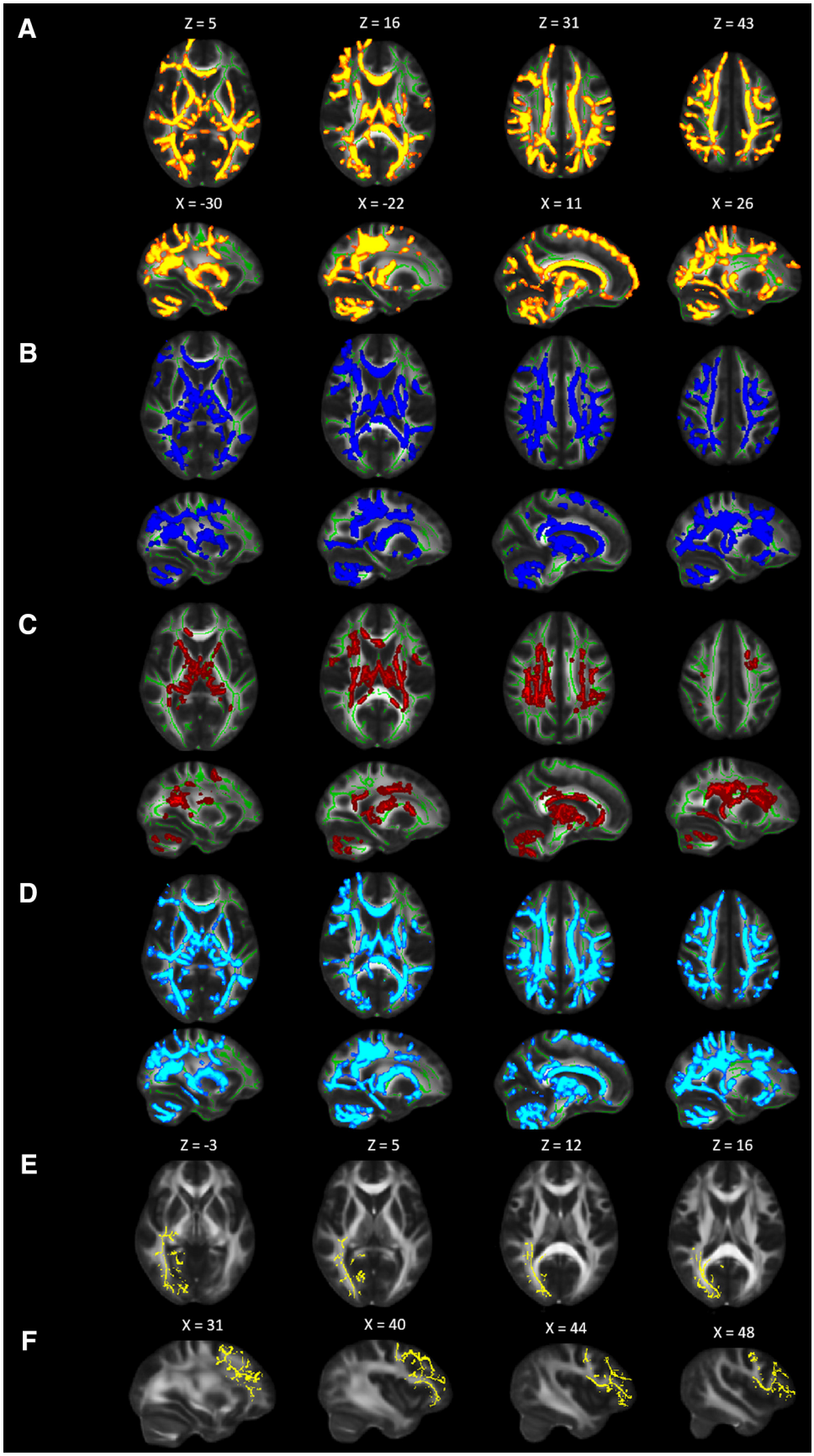

Figure 2. Diffusion tensor metrics demonstrate that WM microstructure is compromised by brain tumor treatment. Widespread differences in WM diffusion metrics between healthy children and brain tumor patients as demonstrated using TBSS. Results are displayed on study-specific WM skeleton (green voxels) and superimposed on FMRIB FA template (slice numbers are in MNI coordinate space). Relative to controls, patients have significant ($p < 0.05$). ***A***, decreased FA (one cluster = 75,259 voxels) depicted in red-yellow. Increased (***B***) MD (*Figure legend continues.*)

our PLS–path modeling is proposed as the geometric mean of the average communality and the average R^2. We used the following guidelines for judging a good fit: GoF > 0.36 (Tenenhaus et al., 2005); bootstrap percentile confidence intervals for path weights (β; 95% percentile), and R^2 did not contain zero.

Computational modeling

Corticocortical network model. We developed a simplified population-scale network model of the corticocortical (V1 and cuneus) system in which task-related presynaptic inputs, both feedback and recurrent, are delivered with timings that are dependent on the integrity of the solicited WM pathways. These task-related inputs are expected to trigger a phase reset of ongoing oscillations. The model consists of both V1 (V1) and cuneus (V5) networks, whose activity obeys the set of coupled Wilson–Cowan equations (Wilson and Cowan, 1972):

$$\alpha_e^{-1}\frac{d}{dt}U_{e,v1}(t) = -U_{e,v1}(t) + w_{e,e}f[U_{e,v1}(t)] + w_{i,e}f[U_{i,v1}(t)] + I(t_o) + \sqrt{2D}\xi_{e,v1}(t)$$

$$\alpha_i^{-1}\frac{d}{dt}U_{i,v1}(t) = -U_{i,v1}(t) + w_{e,i}f[U_{e,v1}(t)] + w_{i,i}f[U_{i,v1}(t)] + I(t_o) + \sqrt{2D}\xi_{i,v1}(t)$$

$$\alpha_e^{-1}\frac{d}{dt}U_{e,v5}(t) = -U_{e,v5}(t) + w_{e,e}f[U_{e,v5}(t)] + w_{i,e}f[U_{i,v5}(t)] + w_{e,v5}f[U_{e,v1}(t-\tau)] + I(t_o) + \sqrt{2D}\xi_{e,v5}(t)$$

$$\alpha_i^{-1}\frac{d}{dt}U_{i,v5}(t) = -U_{i,v5}(t) + w_{e,i}f[U_{e,v5}(t)] + w_{i,i}f[U_{i,v5}(t)] + w_{e,v5}f[U_{e,v1}(t-\tau)] + I(t_o) + \sqrt{2D}\xi_{i,v5}(t),$$

where the mean-activity of excitatory ($U_{e,v1}$) and inhibitory ($U_{i,v1}$) cortical neurons in V1 are coupled with the activity of both excitatory ($U_{e,v5}$) and inhibitory ($U_{i,v5}$) cuneus populations. A propagation delay τ between V1 and cuneus was estimated based on the activity onset time in the data. The activity of each population evolves according to a combination of noise and synaptic inputs. Parameters were set to the values commonly used in the computational neuroscience literature in which Wilson–Cowan networks are used model cortical populations (see model parameters in Table 2; Brunel and Wang, 2003; Wallace et al., 2011; Jadi and Sejnowski, 2014).

The nonlinear activation function f determines the response of a population to recurrent inputs from other populations, as is defined as the sigmoid $f[U] = (1+\exp[-\beta(U-h)])^{-1}$. As defined above and for chosen parameters, the network exhibits sustained beta activity with arbitrary phase. Both V1 and cuneus populations are subjected to an intrinsic source of noise of intensity D and task-related input $I(t_o) = I_o\sum_k \delta(t_o + \tau_k)$, which is a series of K input pulses of intensity I_o delivered at times $t_o + \tau_k$, where t_o is the task cue onset time, and τ_k are random latencies sampled from a gamma distribution $\Gamma 1(\alpha, \theta)$. These inputs can be thought of as representing various networks sharing functional connections with the modeled network and also involved in the task. In addition, to take into account the potential myelin damage between V1 and cuneus, the propagation delay τ was also changed in every trial and set to $\tau + \tau_k$, where the additional latencies τ_k were also sampled from a gamma distribution $\Gamma 2(\alpha, \theta)$.

Brain damage is believed to hinder neural communication through axonal demyelination and axonal neural damage, which triggers conduction failure and/or delayed propagation between and within brain areas. To represent this in our model, brain damage was assessed by an increase in the order of the gamma distribution from which input timings are sampled. This translates into an increase of input timing dispersion as damage increases (i.e., propagation latencies become more variable). We analyzed the phase-locking statistics of the model across fully independent trials, and investigated the influence of task-dependent inputs timing dispersion on the results. Phase-locking was computed using the same method as the human MEG data.

Results

Visual-motor reaction time is slowed in children treated for BTs

Information processing speed was quantified as the reaction time to a go stimulus in our visual-motor task (see Materials and Methods). Healthy children were significantly faster in pressing the button in response to the visual cue: mean reaction time healthy children (312.33 ± 48.87 ms SD) versus BT patients (349.04 ± 44.36 ms SD; $t_{(2,50)} = -2.97$, $p = 0.005$, two-sample t test).

WM microstructure is compromised in children treated for BTs

To compare WM microstructure between groups, we used a voxelwise approach to test for group differences in DTI indices across the entire brain. Healthy children displayed higher FA, lower MD, AD, and RD across the brain compared with children treated for a BT (Fig. 2*A–D*). We then isolated WM within OR/V1/cuneus for the right and left hemispheres (Fig. 2*E*) and extracted mean FA, RD, MD, and AD separately for each hemisphere. Multivariate ANOVA was used to compare healthy children versus BT patients across all DTI indices within the left and right regions of WM and an effect of group was observed (Wilks $\Lambda = 0.62$, $F_{(4,46)} = 7.14$, $p < 0.001$, MANOVA). Healthy children had significantly greater FA, and lower MD, AD, and RD than patients within the WM bilaterally (Table 1). The largest effect size for group differences in WM was, in decreasing order, RD ($\eta^2 = 0.34$), MD ($\eta^2 = 0.31$), FA ($\eta^2 = 0.24$), and AD ($\eta^2 = 0.18$). Only the top three indices were carried forward to our path model.

Neural activation and phase synchrony is perturbed in children treated for BTs

Event-related beamformer analysis revealed early visual areas involved in attention from 0 to 200 ms after the attention cue. In Figure 3*A*, significant ($p < 0.01$) group-averaged source activity for the attention cue (latency 100–200 ms) is presented and plotted on template glass-brain plots and inflated cortical group mesh models. The only activations seen in both groups were within the right primary visual cortex and right cuneus.

We then evaluated neural responses for each participant using anatomically predefined ROIs for primary visual cortex and cuneus. We chose this approach rather than whole-brain thresholding methods to avoid overlooking differences in weakly activated areas. The cortical onset for controls were as follows: V1, 79.2 ms; cuneus, 80.0 ms; and for patients: V1, 80.8 ms; cuneus, 81.7 ms. These results demonstrate a sequence of neural events for both groups from primary visual cortex to cuneus during the visual attention phase of our task (Fig. 3*B*).

Using these predefined ROIs, task-driven PLF was computed between 1 and 60 Hz within V1 and cuneus for each participant. PLF reflects the variability of oscillatory activity across multiple trials at a particular time-frequency point (Tallon-Baudry et al., 1996) and is scaled from "0" reflecting no phase synchrony to "1" reflecting perfectly synchronized phases (Schack and Klimesch,

←

(*Figure legend continued.*) (one cluster = 54971 voxels) shown in blue, (***C***) AD (six clusters = 21,912 voxels) shown in blue, and (***D***) RD (one cluster = 73,101 voxels) shown in cyan. ***E***, Axial view of right cuneus, V1, and OR mask (12,306 voxels). ***F***, Sagittal view of right frontal mask (12,628 voxels). Images are in radiological convention. Numbers represent MNI coordinates.

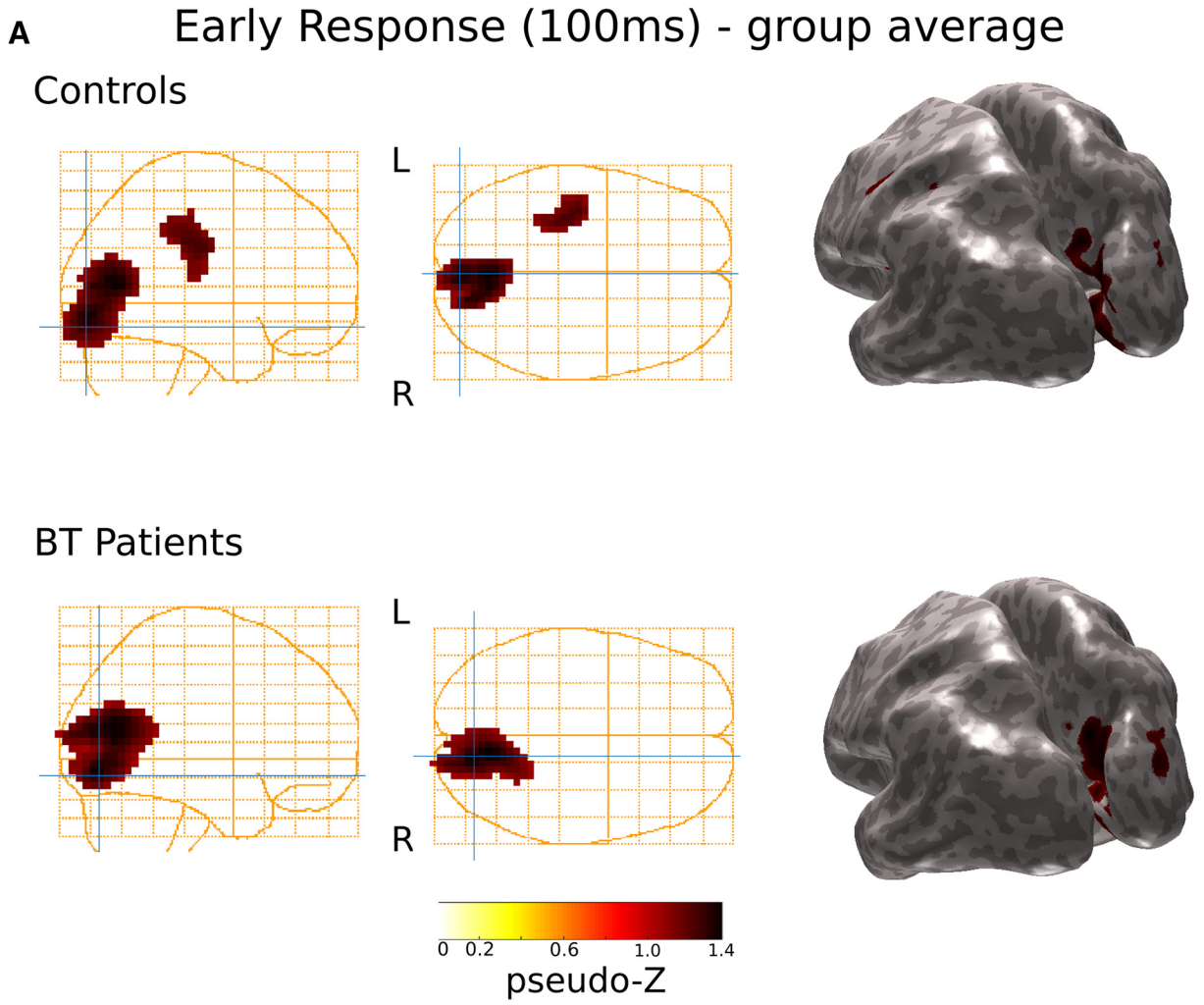

Figure 3. Task-driven activation within V1 precedes cuneus synchrony for controls and children treated for brain tumor. ***A***, Group activation (source power) following visual cue using event-related Synthetic Aperture Magnetometry (pseudo-Z, 1–60 Hz, $p < 0.001$) show activation within V1 and cuneus as represented on glass brain plots and inflated cortical mesh models for (top) controls ($n = 26$) and (bottom) patients treated for BT ($n = 26$). ***B***, Plots representing the activation timing within V1 (blue trace) and cuneus (red trace) for controls and patients with their corresponding standard error (SE) at each time point.

2002). Group-averaged PLF plots for V1 and cuneus were created (Fig. 4*A*) and from the plot it can be seen that the peak PLF for both groups and areas occurs between 100 and 200 ms. Healthy children showed robust right V1 and cuneus phase-locking to the attend cue from 100 to 200 ms in alpha (8–15 Hz), beta (16–29 Hz), and gamma (30–60 Hz), whereas patients demonstrated weaker phase-locking in those frequency bands. There were no differences between groups in number of trials used in PLF calculations ($t_{(2,50)} = -0.59$, $p = 0.56$, two-sample t test). Neither group showed substantial phase-locking in the delta (2–4 Hz) or theta (5–7 Hz) bands. For each participant, peak PLFs were extracted across the different frequency bands for the two ROIs. Mean PLF across all frequencies between 100 and 200 ms differed between healthy children and BT patients (0.42 ± 0.18 vs 0.36 ± 0.18; $F_{(1,50)} = 6.60$, $p = 0.01$, ANOVA). PLF differed across frequency band as well ($F_{(4,50)} = 24.20$, $p = 0.01$, ANOVA). Tests of simple effects revealed that healthy children had significantly greater PLF in cuneus theta ($F_{(1,50)} = 5.26$, $p = 0.03$) and alpha ($F_{(1,50)} = 7.92$, $p = 0.007$), and V1 alpha ($F_{(1,50)} = 7.04$, $p = 0.01$, beta ($F_{(1,50)} = 7.07$, $p = 0.01$), and gamma ($F_{(1,50)} = 8.26$, $p = 0.006$) compared with patients. Thus, peak PLFs from theta and alpha bands for cuneus, and alpha, beta, and gamma bands for V1 were carried forward to our path model.

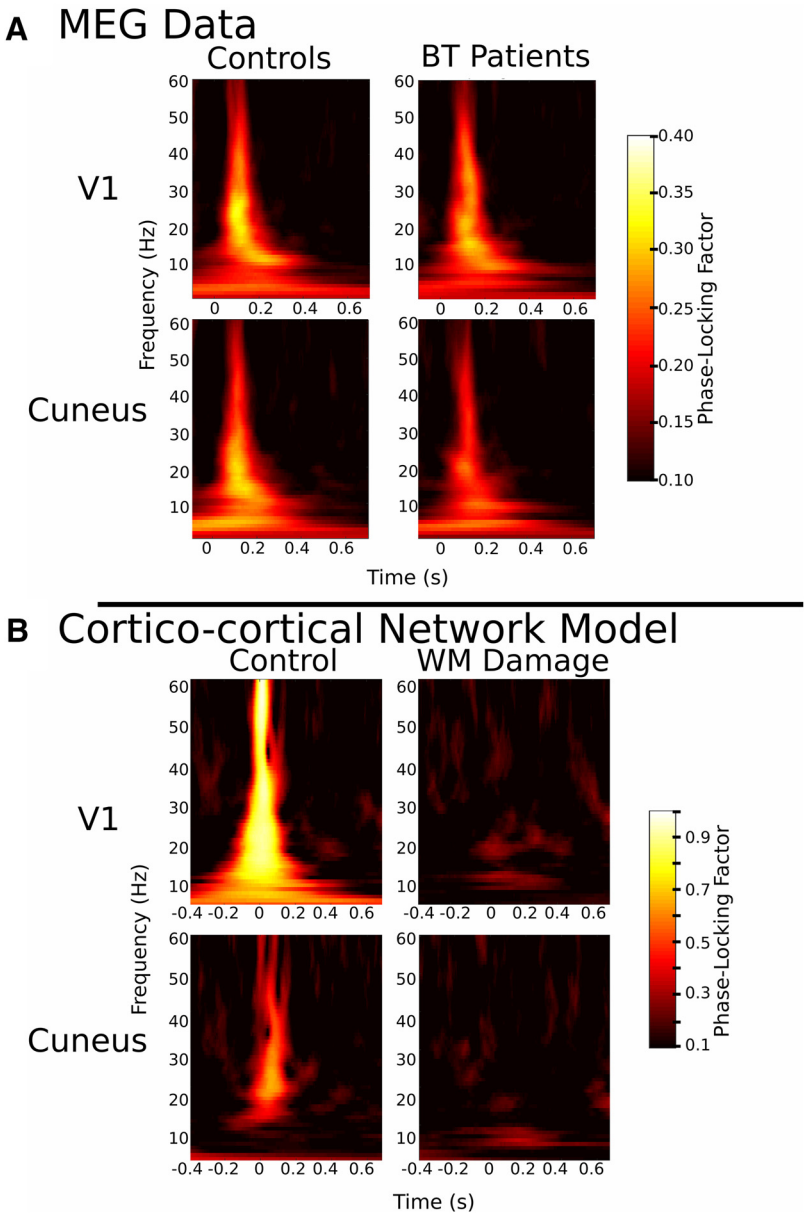

Figure 4. Time/frequency plots of phase-locking factor. ***A***, MEG data: group PLF plots for controls and patients treated for BT for VI (top) and cuneus (bottom) are shown. Patients show reduced phase-locking compared with controls. ***B***, Cortical-cortical model: PLF plots for control model and WB damage model for V1 (top) and cuneus (bottom) are shown.

WM microstructure influences reaction time via effects on neural synchrony

We then tested the relations between WM microstructure and phase synchrony in predicting reaction time using PLS–path model analysis (Sanchez, 2013). In our hypothesized model we suggest that the effects of treatment for a BT on reaction time is mediated by the impact of right OR/V1/cuneus microstructure on neural synchronization in right visual cortex (Fig. 5*A*). We constrained our hypothesized path model to have DTI indices within right OR/V1/cuneus to predict right V1 synchrony as this reflects the anatomic proximity of these structures, additionally to have right V1 predict right cuneus synchrony as this reflects the timing sequence of activation in this early visual response (Fig. 3*B*; Simpson et al., 2011). In our comparison model we hypothesize the effects of treatment for a BT on reaction time is not mediated by the impact of frontal region microstructure (region B; Fig. 2*F* shows mask) on neural synchronization (Fig. 5*B*). The difference between our two models is that within our comparison model we predict DTI indices within frontal regions do not influence V1 synchrony, whereas DTI indices within ORs, V1, and cuneus influence V1 synchrony. In addition to group status (i.e., patients vs healthy children), reaction time, diffusion WM indices along the OR, V1, and cuneus and frontal regions, and phase-locking within V1 and cuneus, we also included age and sex as variables in the model. Age and sex were included as they are known to influence reaction time (Dykiert et al., 2012). In particular, we tested whether MEG measures of neural synchrony had a mediating relationship between WM measures and reaction time (number of bootstraps = 5000).

First, we tested the accuracy of a measurement model that included the following latent constructs: participant (indicators are age, sex, and group status), WM (indicators are FA; note FA loading on the latent variable was changed to be similar as the other DTI indices), RD and MD (within the ORs, V1, and cuneus and frontal regions), V1 (indicators are peak PLF values for alpha, beta, and gamma frequency bands), cuneus (indicators are peak PLF values for alpha, beta, and gamma frequency bands), and reaction time, where reaction time was the outcome variable. All indicators had a loading >0.8 on their respective latent constructs, except age and gender where loadings were 0.4 and 0.2,

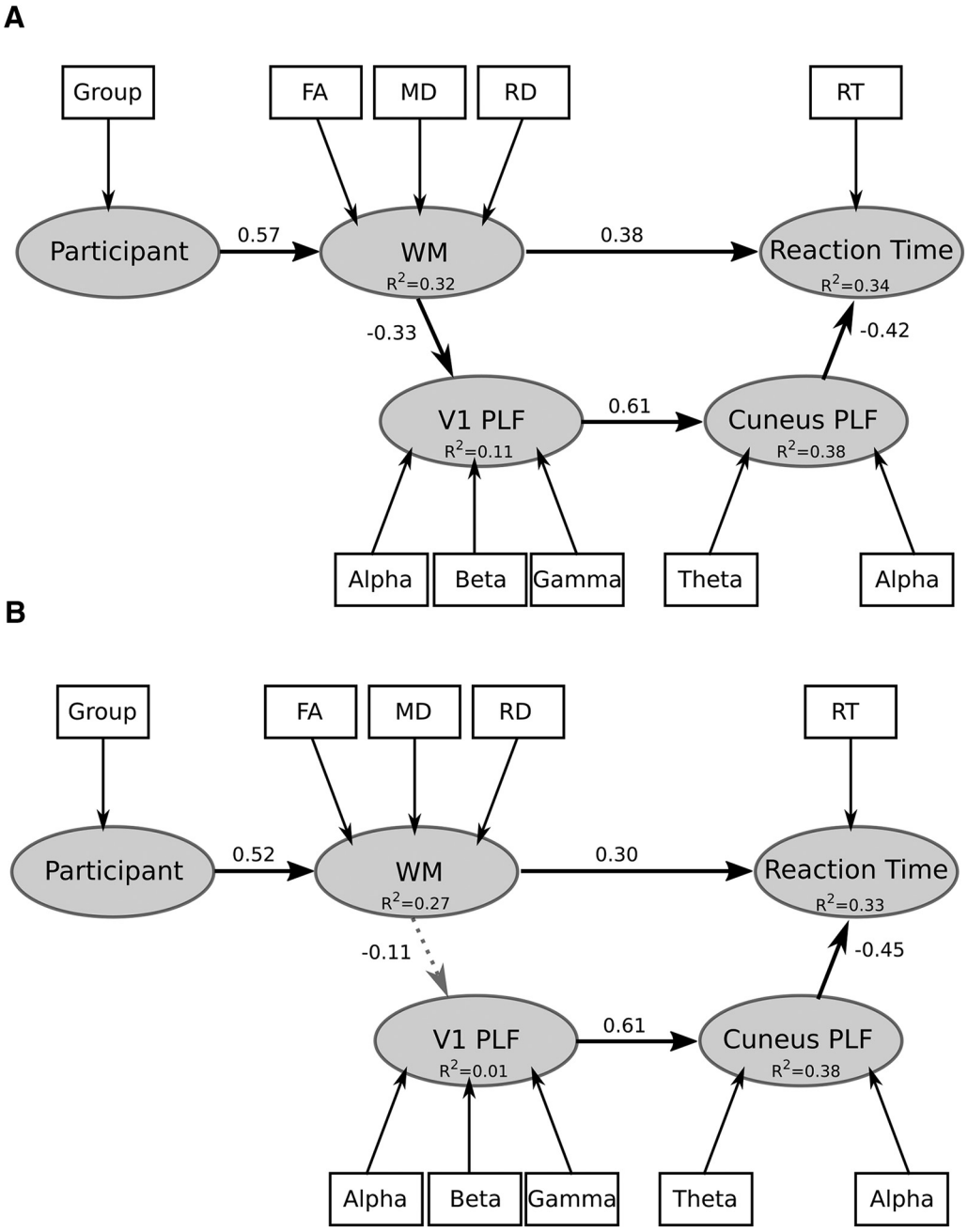

Figure 5. PLS Path model of the relations between treatment for BT, WM measures, phase-locking, and behavioral reaction time. ***A***, Hypothesized path model where we predict the effect of BT treatment on reaction time is mediated (interaction) by the impact of WM microstructure within the OR, V1, and cuneus using DTI indices on synchrony of neural oscillations. ***B***, Control model where we predict the effect of BT treatment on reaction time is not mediated by WM within the frontal lobe on synchrony of neural oscillations.

respectively. Hence, these measures were removed from the model. All remaining measures corresponded well with their latent constructs (Cronbach's alpha >0.85, Dillon–Goldstein's rho >0.9). Further, the discriminant validity of the measurement model was good: cross-loading for each measure relative to the other latent constructs were larger (>0.1) than the loadings obtained from measures belonging to other latent constructs. In essence, indicators should correlate strongly with the latent construct it is associated with and weakly with other latent constructs otherwise it is impossible to discriminate whether the indicator in question belongs to its intended latent construct or to another.

As shown in Figure 5*A*, we observed within our hypothesized model that participant predicted WM [$\beta = 0.57$ (CI_{95}: 0.41, 0.71), $t = 4.84$, $p < 0.001$], WM predicted V1 [$\beta = -0.33$ (CI_{95}: −0.51, −0.13), $t = -2.44$, $p < 0.02$] and reaction time [$\beta = 0.38$ (CI_{95}: 0.18, 0.57), $t = 2.42$, $p < 0.002$], V1 predicted cuneus [$\beta = 0.61$ (CI_{95}: 0.45, 0.76), $t = 5.51$, $p < 0.001$], and cuneus predicted reaction time [$\beta = -0.42$ (CI_{95}: −0.6, −0.24), $t = -3.51$, $p < 0.001$]. Coefficients of determination (R^2) for each latent variable are as follows: WM = 0.32 (CI_{95}: 0.17, 0.5), V1 = 0.11 (CI_{95}: 0.02, 0.26), cuneus = 0.38 (CI_{95}: 0.17, 0.54), and reaction time = 0.34 (CI_{95}: 0.17, 0.54). The indirect effect of WM on reaction time through V1 and cuneus neural synchrony was significant [$\beta = 0.1$ (CI_{95}: 0.04, 0.16)]: increased RD or MD, or decreased FA, predicted reduced phase-locking. In turn, reduced phase-locking

predicted increased reaction time. The GoF measure for our PLS path modeling was 0.49. Aves were 0.84, 0.82, and 0.82 for WM, cuneus, and V1, respectively, which were all larger than the recommended 0.5 cutoff (Sanchez, 2013) and greater than the correlations between constructs (<0.80). In the comparison model in Figure 5*B*, we observed that participant predicted WM [β = 0.52 (CI_{95}: 0.36, 0.67), $t = 4.23$, $p < 0.001$], WM did not predict V1 [$\beta = -0.11$ (CI_{95}: −0.38, 0.17), $t = -0.77$, $p = 0.4$], and WM predicted reaction time [$\beta = 0.3$ (CI_{95}: 0.1, 0.53), $t = 2.3$, $p < 0.005$]; V1 predicted cuneus [$\beta = 0.61$ (CI_{95}: 0.46, 0.77), $t = 5.49$, $p < 0.001$] and cuneus predicted reaction time [$\beta = -0.45$ (CI_{95}: −0.61, −0.26), $t = -3.74$, $p < 0.005$]. Coefficients of determination (R^2) for each latent variable is as follows: WM = 0.27 (CI_{95}: 0.13, 0.45), V1 = 0.01 (CI_{95}: 0.0, 0.14), cuneus = 0.38 (CI_{95}: 0.21, 0.59), and reaction time = 0.33 (CI_{95}: 0.17, 0.53). The coefficient of determination of latent variable of V1 synchrony for this model includes 0 and does not pass significant, furthermore the indirect effect of WM on reaction time through V1 and cuneus neural synchrony was not significant [$\beta = 0.012$ (CI_{95}: 0.0, 0.1)]: increased RD or MD, or decreased FA, within frontal WM does not predict phase-locking. We also conducted the PLS–path modeling using a more restricted ROI which included only the WM underlying the areas of V1 and cuneus MEG activation. When we applied this ROI, the model parameters were largely unchanged. Thus, treatment with radiation has direct and indirect effects on behavioral reaction time, via the impact of OR, V1, and cuneus microstructure on neural synchronization within early visual response.

Computational models replicate reduced neural synchronization by increasing dispersion of action potential conduction latencies

According to on our PLS–path model, WM microstructure appears to play an important role in propagating signals in such a manner as to produce synchronous neural oscillations and efficient cognitive processing. To better understand the underlying biophysical mechanisms, we used computational modeling to assess the impact of an increase in the variance of conduction velocity, which we hypothesize to result from changes in WM microstructure (Siegel et al., 2012), on cortical-cortical oscillations. Disruption of conduction velocity will increase the dispersion of task-related inputs to cortex; therefore, we examined the effect of asynchronous recruitment on the phase-locking of oscillatory activity within a V1 and cuneus network and across independent trials. As shown in Figure 4*B*, our simulations indicate that increased dispersion of the input timings reliably suppresses phase resets and thus robustly hinders the coherence of task-related oscillations. Our simulation also showed a strong dependence of broadband phase-locking on the level of intrinsic noise present within both V1 and cuneus cortical populations. Indeed, for both networks, the robustness of phase-locking was compromised more significantly in the damaged condition, compared with the control condition. Together, these observations support the idea that phase coherence across trials reflects the synchrony of task-related inputs and is thus strongly dependent on both the microstructure of WM pathways and the level of noise shaping the dynamics of neural populations.

Discussion

Using multimodal neuroimaging and computational modeling we provide novel evidence that local WM microstructure affects the cognitive operation of information processing speed through its influence on local neural phase synchrony. Our main findings are as follows: (1) patients show evidence of delayed reaction time, WM compromise, and reduced phase synchrony during visual attention; (2) differences in FA, RD, and MD between patients and healthy children within the optic radiations, V1 and cuneus predict VI and cuneus phase synchrony to a visual event which, in turn, predicts behavioral reaction time; (3) differences in FA, RD, and MD between patients and healthy children within the frontal lobe does not predict V1 and cuneus phase synchrony to a visual event; and (4) in a simple computational model of WM insult, disruption of the timing (synchrony) of neural inputs disrupts phase coherence.

Few studies have investigated the links between WM microstructure, neural function, and cognition, and recent reviews further highlight the need for exactly such work (Fields, 2015; Nunez et al., 2015). The characteristics of our clinical sample make it an excellent population in which to examine these relationships. First, our DTI findings are consistent with previous work showing that patients treated for BT display lower FA and greater RD and MD relative to healthy children, indicative of WM compromise (Mabbott et al., 2006; Law et al., 2015). Indeed, many studies have demonstrated that demyelination and/or axonal damage arising from different causes are reflected by changes in RD, MD, and FA values (Alexander et al., 2007). Second, compared with healthy children, patients exhibited decreased phase synchrony within the alpha, beta, and gamma frequency bands within V1 and cuneus during visual attention. Phase synchrony in these regions likely reflects attention and top-down neural communication within frontal-parietal network on visual attention processing (Yamagishi et al., 2008). In particular, phase-locking in the low-frequency bands (1–10 Hz) has been previously shown to be associated with higher levels of performance during visual tasks (Yamagishi et al., 2008), attentional processes (Ding et al., 2006), and inter-region or long-range communication (von Stein and Sarnthein, 2000). Phase-locking in the gamma band (26–60 Hz) is associated with increased attention and visuo-motor learning (Fries et al., 2001; Perfetti et al., 2011), but also with intra-region or local processing (Yamagishi et al., 2008). Finally, the slower reaction times we observed in patients during a visual-motor task corroborate our previous results (Scantlebury et al., 2016). Reduction of information processing speeds, often manifest as slowed reaction times, are one of the most common cognitive impairments in various clinical populations with WM abnormalities (Filley, 2005). By comparing such a clinical population to healthy children, we were able to reveal differences within WM, neural synchrony, and information processing, providing the platform to model the impact of myelin damage on neural oscillations and cognition.

Myelin, which speeds up action potential propagation by insulating axons, is critical in the regulation of synchronous activity between neurons (Lang and Rosenbluth, 2003). It has been proposed that damage to myelin, axons, and/or axon membrane alters conduction velocities and decreases temporal synchrony within neural ensembles by increasing the variance in conduction velocity, resulting in impaired neural function (Pajevic et al., 2014; Fields, 2015; Nunez et al., 2015). We observed that variations in DTI indices within the OR, V1, and cuneus, reflected as the difference between patients and healthy children, had direct effects on behavioral reaction time and indirect effects through visual cortex synchrony. In comparison DTI indices within the frontal lobe did not have an effect on visual cortex synchrony. Based on these findings we conclude that WM within the OR, V1, and cuneus plays a contributing factor to phase synchrony within

the visual pathway, which in turn is linked to information processing speed.

We further explored the impact of WM microstructure compromise on neuronal synchrony by developing a simplified population-scale network model of a corticocortical system in which task-related inputs, both feedback and recurrent, were delivered with disturbed timings that reflected WM damage. Our simulations indicated that increased dispersion of input timings and intrinsic noise reliably suppressed broadband phase resets in cortical populations and thus robustly hindered the coherence of task-related oscillations. Furthermore, for both networks, decreased phase-locking was found in the damaged condition. We note the striking similarity in the effects of WM damage on PLF between the human and computational data (Fig. 4*A*,*B*). Together our human and modeling data suggest that the decrease in phase-locking we observed within our patient population may be the result of disruptions in the phase reset of local neural oscillators, due to disrupted input timing consequent to local WM insult, yielding asynchronous firing during attentional control, which in turn perturbed the speed of behavioral response in a visual motor reaction time task. That is, the disruption of phase coherence across trials that we observed reflects inconsistency in the timing of task-related inputs predicted by WM microstructure compromise and the level of noise shaping the dynamics of neural populations.

A limitation of our study is that patients had variable medical histories. In addition to tumor type, patients showed heterogeneity in the number of surgeries, chemotherapy treatments, and the number, location, and CRT doses. Although CRT is commonly correlated with WM compromise and cognitive impairments, other medical and treatment variables can influence WM architecture (Malone et al., 2015). Indeed, patients treated for low-grade gliomas, in the absence of CRT, show WM compromise and slowed information processing (Liu et al., 2015). However, despite this heterogeneity, patients collectively show a robust change in WM microstructure leading to reduced phase synchrony in visual processing and, in turn, slowed information processing speeds. This suggests that despite differences in the cause of microstructural changes in WM, there are changes revealed by DTI that translate into a effect on neural function. Future directions with patient populations include increasing the sample sizes for various subgroups (i.e., surgery-only, surgery/chemotherapy-only, focal radiation) and conducting multiple regressions to apply to path models using patient characteristics as independent variables. Finally, here we examined local synchronization within regions and not between regions. Future work examining intra-regional synchronization will allow direct evaluation of the impact of WM damage on large-scale neural communication.

Conclusion

Cognition is the product of coordinated firing of neuronal assemblies (Fries, 2005). WM is composed of axons, dendrites, and glial cells. Glial cells in particular myelinate axons and thereby facilitate the speed and coordination of action potential propagation along neuronal fibers and among neurons (Waxman, 1980; Salami et al., 2003). Understanding how WM microstructure affects cognition is critical for understanding the neural basis of normal cognition and its pathological disruption in a broad range of disorders. Other mechanisms are undoubtedly involved in linking WM microstructure to cognition but this is, to our knowledge, the first study to demonstrate the links between WM architecture, neural synchrony, and information processing speed. Specifically, we show that WM microstructure within the OR, V1, and cuneus influences neural synchrony within the visual cortex and the speed of information processing on a visual-motor task. WM compromise has an indirect adverse impact on information processing via perturbed phase synchrony. We show that when diffusion measures are used in concert with measures of neural function they can provide information on how the relationships between WM microstructure and real-time neural function manifest into cognitive performance. Uniquely, we corroborate these results using a corticocortical computational model showing that input timing dispersion of neuronal signals, representing perturbed signal conduction from myelin damage, disrupts phase coherence in a neuronal network. Together, these findings motivate us to propose that regional neuronal communication is implemented by the synchronization within multiple frequency bands among local neural groups, whereby changes of phases are modulated by local WM microstructure which in turn affects cognitive processing.

References

Alexander AL, Lee JE, Lazar M, Field AS (2007) Diffusion tensor imaging of the brain. Neurotherapeutics 4:316–329. CrossRef Medline

Ashburner J (2009) Computational anatomy with the SPM software. Magn Reson Imaging 27:1163–1174. CrossRef Medline

Basser PJ, Mattiello J, LeBihan D (1994) Estimation of the effective self-diffusion tensor from the NMR spin echo. J Magn Reson B 103:247–254. CrossRef Medline

Bethune A, Tipu V, Sled JG, Narayanan S, Arnold DL, Mabbott D, Rockel C, Ghassemi R, Till C, Banwell B (2011) Diffusion tensor imaging and cognitive speed in children with multiple sclerosis. J Neurol Sci 309:68–74. CrossRef Medline

Brunel N, Wang XJ (2003) What determines the frequency of fast network oscillations with irregular neural discharges? I. Synaptic dynamics and excitation-inhibition balance. J Neurophysiol 90:415–430. CrossRef Medline

Cheyne D (2012) BrainWave software. Toronto, ON: The Hospital for Sick Children.

De Moraes CG (2013) Anatomy of the visual pathways. J Glaucoma 22:S2–S7. CrossRef Medline

Ding J, Sperling G, Srinivasan R (2006) Attentional modulation of SSVEP power depends on the network tagged by the flicker frequency. Cereb Cortex 16:1016–1029. CrossRef Medline

Dockstader C, Gaetz W, Rockel C, Mabbott DJ (2012) White matter maturation in visual and motor areas predicts the latency of visual activation in children. Hum Brain Mapp 33:179–191. CrossRef Medline

Dockstader C, Wang F, Bouffet E, Mabbott DJ (2014) Gamma deficits as a neural signature of cognitive impairment in children treated for brain tumors. J Neurosci 34:8813–8824. CrossRef Medline

Dubois J, Dehaene-Lambertz G, Soarès C, Cointepas Y, Le Bihan D, Hertz-Pannier L (2008) Microstructural correlates of infant functional development: example of the visual pathways. J Neurosci 28:1943–1948. CrossRef Medline

Dykiert D, Der G, Starr JM, Deary IJ (2012) Sex differences in reaction time mean and intraindividual variability across the life span. Dev Psychol 48:1262–1276. CrossRef Medline

Ferguson AN, Bowey JA (2005) Global processing speed as a mediator of developmental changes in children's auditory memory span. J Exp Child Psychol 91:89–112. CrossRef Medline

Fields RD (2015) A new mechanism of nervous system plasticity: activity-dependent myelination. Nat Rev Neurosci 16:756–767. CrossRef Medline

Filley CM (2005) White matter and behavioral neurology. Ann N Y Acad Sci 1064:162–183. CrossRef Medline

Fries P (2005) A mechanism for cognitive dynamics: neuronal communication through neuronal coherence. Trends Cogn Sci 9:474–480. CrossRef Medline

Fries P, Reynolds JH, Rorie AE, Desimone R (2001) Modulation of oscillatory neuronal synchronization by selective visual attention. Science 291:1560–1563. CrossRef Medline

Garcés P, Angel Pineda-Pardo J, Canuet L, Aurtenetxe S, López ME, Marcos A, Yus M, Llanero-Luque M, Del-Pozo F, Sancho M, Maestú F (2014)

The default mode network is functionally and structurally disrupted in amnestic mild cognitive impairment: a bimodal MEG-DTI study. Neuroimage Clin 6:214–221. CrossRef Medline

Hindriks R, Woolrich M, Luckhoo H, Joensson M, Mohseni H, Kringelbach ML, Deco G (2015) Role of white-matter pathways in coordinating alpha oscillations in resting visual cortex. Neuroimage 106:328–339. CrossRef Medline

Jadi MP, Sejnowski TJ (2014) Cortical oscillations arise from contextual interactions that regulate sparse coding. Proc Natl Acad Sci U S A 111: 6780–6785. CrossRef Medline

Kail R (2000) Speed of information processing: developmental change and links to intelligence. J Sch Psychol 38:51–61. CrossRef

Konrad A, Vucurevic G, Musso F, Stoeter P, Winterer G (2009) Correlation of brain white matter diffusion anisotropy and mean diffusivity with reaction time in an oddball task. Neuropsychobiology 60:55–66. CrossRef Medline

Lachaux JP, Rodriguez E, Martinerie J, Varela FJ (1999) Measuring phase synchrony in brain signals. Hum Brain Mapp 8:194–208. CrossRef Medline

Lang EJ, Rosenbluth J (2003) Role of myelination in the development of a uniform olivocerebellar conduction time. J Neurophysiol 89:2259–2270. CrossRef Medline

Law N, Greenberg M, Bouffet E, Laughlin S, Taylor MD, Malkin D, Liu F, Moxon-Emre I, Scantlebury N, Skocic J, Mabbott D (2015) Visualization and segmentation of reciprocal cerebrocerebellar pathways in the healthy and injured brain. Hum Brain Mapp 36:2615–2628. CrossRef Medline

Liu F, Scantlebury N, Tabori U, Bouffet E, Laughlin S, Strother D, McConnell D, Hukin J, Fryer C, Brière ME, Montour-Proulx I, Keene D, Wang F, Mabbott DJ (2015) White matter compromise predicts poor intellectual outcome in survivors of pediatric low-grade glioma. Neuro Oncol 17: 604–613. CrossRef Medline

Mabbott DJ, Noseworthy MD, Bouffet E, Rockel C, Laughlin S (2006) Diffusion tensor imaging of white matter after cranial radiation in children for medulloblastoma: correlation with IQ. Neuro Oncol 8:244–252. CrossRef Medline

Mabbott DJ, Snyder JJ, Penkman L, Witol A (2009) The effects of treatment for posterior fossa brain tumors on selective attention. J Int Neuropsychol Soc 15:205–216. CrossRef Medline

Madden DJ, Whiting WL, Huettel SA, White LE, MacFall JR, Provenzale JM (2004) Diffusion tensor imaging of adult age differences in cerebral white matter: relation to response time. Neuroimage 21:1174–1181. CrossRef Medline

Malone IB, Leung KK, Clegg S, Barnes J, Whitwell JL, Ashburner J, Fox NC, Ridgway GR (2015) Accurate automatic estimation of total intracranial volume: a nuisance variable with less nuisance. Neuroimage 104:366–372. CrossRef Medline

Mori S, Oishi K, Jiang H, Jiang L, Li X, Akhter K, Hua K, Faria AV, Mahmood A, Woods R, Toga AW, Pike GB, Neto PR, Evans A, Zhang J, Huang H, Miller MI, van Zijl P, Mazziotta J (2008) Stereotaxic white matter atlas based on diffusion tensor imaging in an ICBM template. Neuroimage 40:570–582. CrossRef Medline

Nazem-Zadeh MR, Bowyer SM, Moran JE, Davoodi-Bojd E, Zillgitt A, Weiland BJ, Bagher-Ebadian H, Mahmoudi F, Elisevich K, Soltanian-Zadeh H (2016) MEG coherence and DTI connectivity in mTLE. Brain Topogr 29:598–622. CrossRef Medline

Nieder C, Andratschke N, Astner ST (2007) Experimental concepts for toxicity prevention and tissue restoration after central nervous system irradiation. Radiat Oncol 2:23. CrossRef Medline

Nunez PL, Srinivasan R, Fields RD (2015) EEG functional connectivity, axon delays and white matter disease. Clin Neurophysiol 126:110–120. CrossRef Medline

Pajevic S, Basser PJ, Fields RD (2014) Role of myelin plasticity in oscillations and synchrony of neuronal activity. Neuroscience 276:135–147. CrossRef Medline

Perfetti B, Moisello C, Landsness EC, Kvint S, Lanzafame S, Onofrj M, Di Rocco A, Tononi G, Ghilardi MF (2011) Modulation of gamma and theta spectral amplitude and phase synchronization is associated with the development of visuo-motor learning. J Neurosci 31:14810–14819. CrossRef Medline

Roberts TP, Khan SY, Blaskey L, Dell J, Levy SE, Zarnow DM, Edgar JC (2009) Developmental correlation of diffusion anisotropy with auditory-evoked response. Neuroreport 20:1586–1591. CrossRef Medline

Salami M, Itami C, Tsumoto T, Kimura F (2003) Change of conduction velocity by regional myelination yields constant latency irrespective of distance between thalamus and cortex. Proc Natl Acad Sci U S A 100: 6174–6179. CrossRef Medline

Sanchez G (2013) PLS path modeling with R. Berkeley: Trowchex Editions.

Scantlebury N, Bouffet E, Laughlin S, Strother D, McConnell D, Hukin J, Fryer C, Laperriere N, Montour-Proulx I, Keene D, Fleming A, Jabado N, Liu F, Riggs L, Law N, Mabbott DJ (2016) White matter and information processing speed following treatment with cranial-spinal radiation for pediatric brain tumor. Neuropsychology 30:425–438. CrossRef Medline

Schack B, Klimesch W (2002) Frequency characteristics of evoked and oscillatory electroencephalic activity in a human memory scanning task. Neurosci Lett 331:107–110. CrossRef Medline

Siegel M, Donner TH, Oostenveld R, Fries P, Engel AK (2008) Neuronal synchronization along the dorsal visual pathway reflects the focus of spatial attention. Neuron 60:709–719. CrossRef Medline

Siegel M, Donner TH, Engel AK (2012) Spectral fingerprints of large-scale neuronal interactions. Nat Rev Neurosci 13:121–134. CrossRef Medline

Simpson GV, Weber DL, Dale CL, Pantazis D, Bressler SL, Leahy RM, Luks TL (2011) Dynamic activation of frontal, parietal, and sensory regions underlying anticipatory visual spatial attention. J Neurosci 31:13880–13889. CrossRef Medline

Singh KD, Barnes GR, Hillebrand A (2003) Group imaging of task-related changes in cortical synchronisation using nonparametric permutation testing. Neuroimage 19:1589–1601. CrossRef Medline

Smith SM, Jenkinson M, Johansen-Berg H, Rueckert D, Nichols TE, Mackay CE, Watkins KE, Ciccarelli O, Cader MZ, Matthews PM, Behrens TE (2006) Tract-based spatial statistics: voxelwise analysis of multi-subject diffusion data. Neuroimage 31:1487–1505. CrossRef Medline

Soria-Pastor S, Gimenez M, Narberhaus A, Falcon C, Botet F, Bargallo N, Mercader JM, Junque C (2008) Patterns of cerebral white matter damage and cognitive impairment in adolescents born very preterm. Int J Dev Neurosci 26:647–654. CrossRef Medline

Sponheim SR, McGuire KA, Kang SS, Davenport ND, Aviyente S, Bernat EM, Lim KO (2011) Evidence of disrupted functional connectivity in the brain after combat-related blast injury. Neuroimage 54:S21–S29. CrossRef Medline

Stephen JM, Coffman BA, Jung RE, Bustillo JR, Aine CJ, Calhoun VD (2013) Using joint ICA to link function and structure using MEG and DTI in schizophrenia. Neuroimage 83:418–430. CrossRef Medline

Stufflebeam SM, Witzel T, Mikulski S, Hämäläinen MS, Temereanca S, Barton JJ, Tuch DS, Manoach DS (2008) A non-invasive method to relate the timing of neural activity to white matter microstructural integrity. Neuroimage 42:710–716. CrossRef Medline

Tallon-Baudry C, Bertrand O, Delpuech C, Pernier J (1996) Stimulus specificity of phase-locked and non-phase-locked 40 Hz visual responses in human. J Neurosci 16:4240–4249. Medline

Tenenhaus M, Vinzi VE, Chatelin YM, Lauro C (2005) PLS path modeling. Comput Stat Data Anal 48:159–205. CrossRef

von Stein A, Sarnthein J (2000) Different frequencies for different scales of cortical integration: from local gamma to long range alpha/theta synchronization. Int J Psychophysiol 38:301–313. CrossRef Medline

Wallace E, Benayoun M, van Drongelen W, Cowan JD (2011) Emergent oscillations in networks of stochastic spiking neurons. PLoS One 6:e14804. CrossRef Medline

Waxman SG (1980) Determinants of conduction velocity in myelinated nerve fibers. Muscle Nerve 3:141–150. CrossRef Medline

Western SL, Long CJ (1996) Relationship between reaction time and neuropsychological test performance. Arch Clin Neuropsychol 11:557–571. CrossRef Medline

Wilson HR, Cowan JD (1972) Excitatory and inhibitory interactions in localized populations of model neurons. Biophys J 12:1–24. CrossRef Medline

Yamagishi N, Callan DE, Anderson SJ, Kawato M (2008) Attentional changes in pre-stimulus oscillatory activity within early visual cortex are predictive of human visual performance. Brain Res 1197:115–122. CrossRef Medline